JAST, Vol. 14, No. 2, pp. 96-105

JAST
Journal of Aerospace Science and Technology

Science Article

Numerical Investigation on Flow Control of a Small Horizontal Axis Wind Turbine Using Dielectric Barrier Discharge Plasma Actuator

Majid Sedghi [1], Roohollah Khoshkhoo [2*]
1-Department of Mechanical Engineering, Isfahan University of Technology
2- Faculty of Mechanical Engineering, Malek Ashtar University of Technology

[*]**Email: r.khoshkhoo@mut.ac.ir**

This research aims to numerically investigate the efficiency of the plasma actuator in a small wind turbine. The studies were conducted on a domestic wind turbine with a diameter of 1.93 m and the Suzen-Huang model was employed to simulate the Dielectric Barrier Discharge (DBD) plasma actuator. In this research, firstly, a wind turbine without the plasma actuator was simulated at different tip speed ratios. Then, the DBD plasma actuator was activated at a tip speed ratio of 4.35, and changes in the power output, torque distribution, and surface streamlines were studied. The results indicate with an increase in the power of the plasma actuator, the separation point moves away from the leading edge, the span-wise flows are reduced, and the turbine power output is increased. The performance of the plasma actuator is varied along the wind turbine blade length. For the radii $r/R = 0.4 - 0.95$, a difference in the generated torque can be observed for active and inactive plasma modes, and the plasma actuator did not significantly affect the power output in other sections. The maximum increase in torque due to the plasma actuator occurred at the radii $r/R = 0.5 - 0.7$. In these regions, the distance between the separation point and the plasma actuator location is about 0.2 times the chord length of the airfoil.

Keywords: *Horizontal axis wind turbine, Flow control, Plasma actuator, Dielectric barrier discharge, Suzen-Huang model*

Nomenclature

C	Chord, $[m]$	y^+	Dimensionless wall distance, $[-]$
C_p	power coefficient, $[-]$	ε_r	relative permittivity, $[-]$
D	rotor diameter, $[m]$	ϕ	electric potential, $[V]$
f_{bi}	body force, $[N/m^3]$	ϕ^{max}	maximum electric potential, $[V]$
P_{out}	turbine output power, $[W]$	λ	tip speed ratio, $[-]$
p	static pressure, $[Pa]$	λ_d	Debye length, $[m]$
Q	Torque, $[N.m]$	ν	Viscosity, $[m^2/s]$
R	rotor radius, $[m]$	ω	rotational speed, $[rad/s]$
t	time, $[s]$	ρ	Fluid density, $[kg/m^3]$
U	wind speed, $[s]$	ρ_c	charge density, $[C/m^3]$
u_i	velocity field component, $[m/s]$	ρ_c^{max}	maximum charge density, $[C/m^3]$

1. Assistant Professor (Corresponding Author)
2. PhD graduate

Received: 12 July 2021
Accepted: 11 Sept. 2021

Introduction

Wind energy is one of the renewable energy sources that its use has grown tremendously. Statistics show that the capacity of wind turbines installed in the world has increased more than 90 % from 2012 to 2017 [1]. According to IEC 61400-2, a wind turbine with a swept area of less than 200 m^2 is called a small wind turbine. These turbines usually have an output power smaller than 50 kW. Small turbines are classified into micro, mid-range, and mini turbines [2].

Many studies have been conducted on methods of controlling wind turbines to improve their aerodynamic performance [3, 4]. Flow control can reduce the boundary layer thickness, and consequently, delays the separation point. The Dielectric Barrier Discharge (DBD) plasma actuator is one of the active flow control methods on wind turbine blades. Plasma actuators offer ultra-light, compact, and robust mechanical architecture, which is economical in terms of actuation power and costs [5]. According to Fig. 1, a DBD plasma actuator consists of two electrodes with a dielectric material embedded between them. When a high A.C. voltage is supplied to the electrodes, an electric field is created, ionizing the surrounding air and moving them toward the embedded electrode. This air flow acts as a body force and moves the fluid surrounding the electrodes. The induced flow improves the flow profile in the boundary layer and delays flow separation. The performance of a plasma actuator depends on numerous parameters, such as the distance between the electrodes, dielectric thickness, frequency, and waveform of the applied voltage [6].

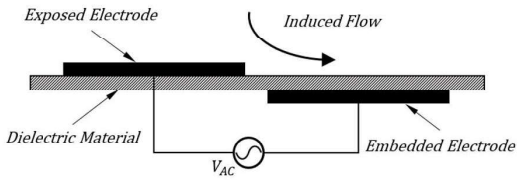

Figure 1. Schematic of a DBD plasma actuator

Extensive research has been conducted to control the flow boundary layer using plasma actuators [7-9]. The experimental research by Jacob et al. [10] indicates that the fluid next to the DBD plasma actuator immediately accelerates, and a turbulent jet is created downstream of the actuator.

Many electro-hydrodynamic models are suggested for modeling plasma actuators, which simulate the generated plasma and the electrical potential field and add the interaction force as a source term to the momentum equation. In the Suzen-Huang model, 2 equations are solved to determine the electric field and the charge density of the ionized air [11-13]. In this model, the Debye length and the maximum charge density are determined based on experimental results. Ibrahim and Skote [14] have studied the effects of changing these two parameters on the generated force and induced speeds of the plasma actuator in the Suzen-Huang model.

Researchers have examined the impact of the thickness, material, and the voltage and frequency applied to the electrodes on the thrust generated by the actuator [15-17]. The results of these studies show that an increase in the electrode thickness reduces the generated thrust. Moreover, an increase in the voltage increases the speed of the induced flow. The electric power consumption of the plasma actuator also increases with an increase in the voltage and current frequency [18].

Hoeijmakers and Meijerink [19] show that, for a wind turbines with NACA-0018 airfoils, it is possible to control the flow up to a Reynolds number of 3.3×10^5 using the plasma actuator. Experimental work of Tanaka et al. [20] on 300-kW wind turbine shows that plasma-actuation technology can effectively control the flow in the $1.6–1.8 \times 10^6$ Re range.

Cooney et al. [21] achieved a power increase of 0.2-1.9% by developing 3 types of plasma actuators for controlling the flow over a 20-kW horizontal axis wind turbine. Rotating stall around a small-scale horizontal axis wind turbine was experimentally investigated by Jukes [22] to characterize and assess the smart rotor control using plasma actuators. He showed that the radial body forces generated by plasma vortex generators are of paramount importance in rotating separated flows. In the experimental research by Matsuda et al. [23], the plasma actuator caused a 4.6% increase in the power generated by a horizontal axis wind turbine with a nominal power of 1.75 MW. They developed plasma electrodes of 8 m in length installed on the surface of the leading edge of each blade.

The numerical simulation results of Ebrahimi and Movahhedi [24] for a 5-MW horizontal axis wind

turbine indicated a 0.85% increase in the output power by the wind turbine after applying the plasma actuator. In their research, Suzen-Huang model was used and a configuration of multi-DBD plasma actuators was located at the inboard part of the blade along the span. Omidi and Mazaheri [25] introduced an improved model based on the Suzen-Huang model. These researchers used this model in another numerical work [26]. They investigated the usage of a plasma actuator to improve the aerodynamic performance of an offshore 6 MW wind turbine. They observed up to 95 kW harvested energy increment by optimization of location and configuration of actuators.

Micro wind turbine can produce enough energy to power the lights and electrical appliances in a typical home. These turbines are commonly used in hybrid photovoltaic-wind systems to supply household electricity. To decide to use a plasma actuator in domestic wind turbines, it is necessary to study the amount of output power increase and the location of the actuator. In the previous works, research focused on wind turbines with power output of several kW to MW and plasma flow control on the domestic small wind turbine received less attention. Therefore, we focus on a 500 W horizontal axis wind turbine. The present research aims to numerically investigate the performance of a DBD plasma actuator on the small wind turbine.

The output power of this wind turbine under different conditions has been derived. At a specific tip speed ratio where the wind turbine has a low power coefficient, the plasma actuator has been applied to the wind turbine blades using the Suzen-Huang model. Changes in the generated power, torque distribution, and streamlines on the wind turbine blades after the activation of the plasma actuator have been discussed.

Reference wind turbine

Given the aim of this research, which is to numerically study the performance of the DBD plasma actuator in a small horizontal axis wind turbine, it is necessary to select a reference wind turbine for performing the simulations. The diameter, twist angle, chord, and airfoil of the blade sections are among the geometric characteristics required for a wind turbine. In addition to geometric characteristics, the rotational speed and the power generation of the wind turbine for various wind speeds are among the items required for validating the results.

In this paper, a 500-W horizontal axis wind turbine has been selected as the reference for the research. Wood et al., have researched on this wind turbine and have presented their results in [2, 27-32]. The diameter of this turbine is 1.93 m, its hub diameter is 0.22 m, and it has 3 blades. The twist and chord distributions of this wind turbine are shown in Table 1. The blade section of this wind turbine consists of the SD7062 airfoil. The availability of experimental data relating to the power output, generator efficiency, and rotational speed of this turbine for various speeds is among the advantages of this wind turbine.

Table 1. Chord and twist angle of different sections along the wind turbine blade

r/R	0.2	0.3	0.4	0.5	0.6	0.7	0.8	0.9	1
C/R	0.185	0.135	0.103	0.084	0.071	0.061	0.054	0.047	0.043
Twist Angle (Deg)	17.2	12.6	9.5	7.6	6.3	5.4	4.7	3.9	3.2

Governing equations

The equations governing the flow are the continuity and momentum equations, expressed as follows for a Newtonian fluid [24].

$$\frac{\partial u_i}{\partial x_i}(\rho) = 0 \tag{1}$$

$$\frac{\partial u_i}{\partial t} + u_j \frac{\partial u_i}{\partial x_j} = -\frac{1}{\rho}\frac{\partial p}{\partial x_i} + \nu \frac{\partial^2 u_i}{\partial x_i x_j} + \frac{\partial \tau_{ij}}{\partial x_i} + f_{bi} \tag{2}$$

where u_i is the velocity field component, p is the static pressure, ρ is the fluid density, ν is the viscosity, and τ_{ij} is called the Reynolds stress. f_{bi} represents the rest of the body forces, which are produced by the plasma actuator in this research.

To compute the body force caused by the plasma actuator, the electric field potential distribution and the charge density distribution are required. In the model proposed by Suzen and Huang [12], equations (3) and (4) have been presented for calculating the electric field potential distribution and charge density distribution, respectively [12]:

$$\nabla.(\varepsilon_r \nabla\phi) = 0 \tag{3}$$

$$\nabla.(\varepsilon_r \nabla\rho_c) = -\frac{\rho_c}{\lambda_d^2} \tag{4}$$

where ε_r denotes the relative permittivity, λ_d represents the Debye length, ϕ is the electric field potential distribution, and ρ_c denotes the charge density distribution in the computational domain. The charge density and the electric potential can be made dimensionless as $\rho_c^* = \frac{\rho_c}{\rho_c^{max}}$ and $\phi^* = \frac{\phi}{\phi^{max}}$, by the maximum charge density (ρ_c^{max}) and the maximum electric potential (ϕ^{max}), respectively. Hence, the dimensionless forms of equations (3) and (4) are as follows [12]:

$$\nabla.(\varepsilon_r \nabla \phi^*) = 0 \quad (5)$$

$$\nabla.(\varepsilon_r \nabla \rho_c^*) = -\frac{\rho_c^*}{\lambda_d^2} \quad (6)$$

The electric field distribution (ϕ) and the charge density distribution (ρ_c) in the computational domain are obtained by numerically solving the above equations. The body force is calculated as follows [12]:

$$\vec{f_b} = \rho_c(-\nabla\phi) = \rho_c^{max}\phi^{max}\rho_c^*(-\nabla\phi^*) \quad (7)$$

In this research, the plasma actuator is simulated in a two-dimensional environment, and the body forces resulting from it are derived in a two-dimensional mesh. A code has been written in MATLAB software, which takes the simulated mesh of the plasma actuator and the wind turbine as input. In the vicinity of the radial position on the wind turbine blade where the plasma actuator will be installed, sections perpendicular to the wind turbine blade are considered at distances equal to the thickness of a cell, and the geometrical coordinates of the nodes making up the airfoils of each section are extracted.

After the leading edge and the trailing edge of the airfoils of each section of the wind turbine blades are recognized, the length and the slope of the chord and the line perpendicular to it are computed; then, the geometrical coordinates of the nodes of the plasma actuator location on each airfoil are determined.

Given the coordinates and the slope of the airfoil surface at the location of the plasma, the cell gird and the vector of the body forces of the plasma actuator are rotated and translated in the two-dimensional environment. Since the mesh of the plasma actuator is different from that of the wind turbine, the computed body forces are calculated on the wind turbine mesh via interpolation. Finally, the body forces corresponding to all the nodes of the wind turbine mesh are reported and are defined in Star CCM software as the source term of the momentum equation.

Numerical solution specifications

In this research, the STAR CCM software has been used for numerical simulations of the fluid flow. In the simulations, the steady pressure base solver and the SIMPLE algorithm were used to couple velocity and pressure, and the second-order upwind method was used to discretize the equations. The flow has been assumed to be incompressible, and the fluid has been considered as the ideal gas. The k-w SST model has been employed to model turbulence. In the inlet boundary, the values 0.01 and 10.0 are assigned to the turbulence intensity and turbulent viscosity ratio, respectively. The boundary layer mesh has been created in such a way that y^+ is about 1, which is the most suitable value for the k-w SST turbulence model. Fig. 2 shows the y^+distribution on the wind turbine blade. The Moving Reference Frame (MRF) method has been utilized to model the flow and to simulate the rotational motion of the wind turbine.

In this research, only one of the wind turbine blades has been simulated by applying periodic conditions, and the forces resulting from the simulation are multiplied by the number of blades. The computational domain is in the form of a 120° section of a cylinder. Velocity and pressure boundary conditions have been used at the inlet and outlet of the wind turbine computational domain, respectively.

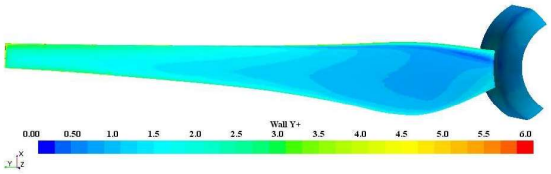

Figure 2. y^+ distribution on the wind turbine blade.

To select the dimensions of the computational domain, the effects of the length of the computational domain on the torque generated by the wind turbine has been studied, and the dimensions presented in Fig. 3 were eventually used in simulations. With a mesh-independence study of the results (Table 2), the mesh with 2 million cells was selected for investigating the performance of the wind turbine without a plasma actuator. Since very small cells are required at the location of the plasma actuator along the blade, the

number of cells for the wind turbine equipped with a plasma actuator has been increased up to 7 million in the present research. Fig. 4 displays the meshing around the blade of the wind turbine equipped with a plasma actuator.

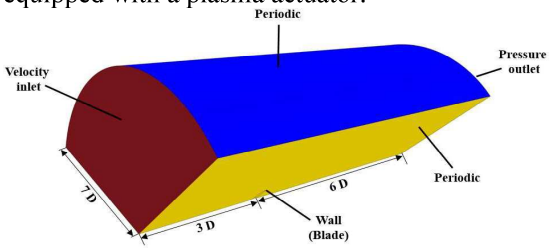

Figure 3. Boundary conditions and dimensions of the computational domain in the simulation of the wind turbine

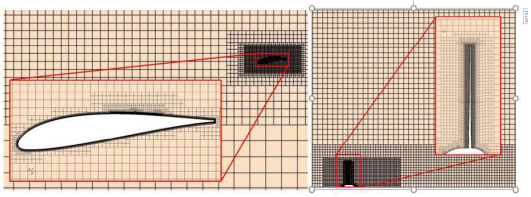

Figure 4. Mesh around the wind turbine blade

Table 2. Effect of the number of mesh cells on the torque generated by the wind turbine

number of cells (× 10^6)	0.463	0.782	1.147	1.512	1.985	2.641
Torque (N.m)	1.770	1.872	1.950	1.992	1.998	2.000

Two dimensionless characteristics, namely the tip speed ratio (λ) and the power coefficient (C_p) are used to study the performance of the wind turbine. These two characteristics are defined as follows:

$$\lambda = \frac{R\omega}{U} \tag{8}$$

$$C_p = \frac{P_{out}}{\frac{1}{2}\rho U^3 \pi R^2} \tag{9}$$

where R is the turbine radius, ω is the turbine rotational speed, U is the wind speed, and P_{out} denotes the wind turbine output power.

Validation of the results

Experimental data relating to the power output, generator efficiency, and rotational speed of the turbine at various wind speeds for the selected wind turbine are available. This wind turbine has been simulated under different conditions, and the computed power generation has been compared to the experimental results in Fig. 5.

A plasma actuator with a specified geometry was studied experimentally by Jacob et al. [33] and numerically by Suzen et al. [13]. In these studies, rectangular electrodes with a length of 10 mm and a thickness of 0.102 mm have been placed at distances of 0.5 mm. A dielectric with a thickness of 0.127 mm and made of Kapton has separated the two electrodes. The Debye length is 0.00017 m, and the maximum charge density is 0.0075 C/m^3. Also, the voltage applied to the electrodes has been considered as 5 kV. One side of the external electrode is in contact with air, and the other side is in contact with the dielectric. When a high A.C. voltage is supplied to the electrodes, the air surrounding the electrode is ionized, and a body force is created. Due to this body force, air is drawn from the surrounding toward the electrodes, and a flow jet is created near the wall from the exposed electrode to the embedded electrode.

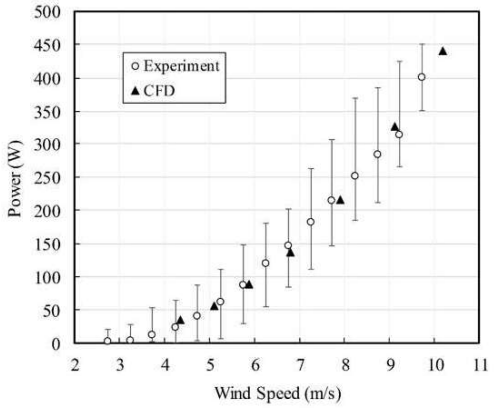

Figure 5. Comparison of the experimental results [27] and the numerical simulation of the power output by the studied wind turbine

The magnitude distribution of the body force computed in the present research has been compared to the research by Suzen et al. [13] in Fig. 6. The region between the two electrodes with the highest plasma effect is shown in these figures. As seen in these figures, a good agreement has been obtained between the contours obtained in the present simulations and the research by Suzen et al. [13].

Results and discussion

In this section, the performance of the wind turbine without a plasma actuator is examined at first. Fig. 7 displays the changes in the power coefficient of the wind turbine at different tip speed ratios. According to this figure, the highest power

coefficient of this wind turbine is at a tip speed ratio of about 6. The power coefficient decreases with an increase or a decrease in λ relative to this point. An increase and a decrease in λ cause a decrease and an increase in the flow angle of attack, respectively.

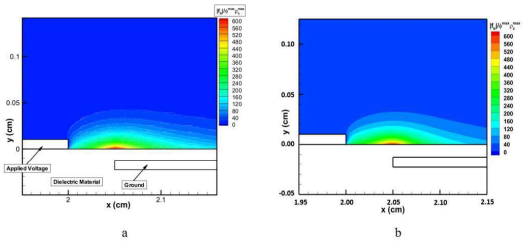

a b

Figure 6. Comparison of the dimensionless body force distribution, a) research by Suzen et al. [13], b) present research

In this research, $\lambda = 4.35$ has been selected for examining the effects of the plasma actuator on the performance of the wind turbine. As shown in Fig. 7, compared to the optimal tip speed ratio, the power coefficient of the wind turbine is low at this tip speed ratio. Fig. 8 shows the surface streamlines on the wind turbine blades and around its airfoils at r/R of 0.2, 0.4, 0.6, and 0.8. According to this figure, as one approaches the wind turbine blade root, the span-wise flow has overcome, and a three-dimensional flow has been created. Flow separation near the leading edge and the presence of wake are among the characteristics of the flow around the airfoils in these regions. As one moves away from the blade roots, the radial velocity ($r\omega$) increases, and the flow angle of attack decreases. A decrease in the angle of attack of the flow near the blade tip causes the separation point to move away from the leading edge of the airfoil. As one approaches the blade tip, the chord-wise flows dominate more areas.

A change in the orderly flow pattern over the surface of the airfoils of the wind turbine blades reduces their optimal aerodynamic performance. In this section, using a plasma actuator, it has been attempted to improve the flow pattern over the airfoil surface and to examine its effect on the performance of the wind turbine.

The plasma actuator used in this research is similar to the actuator used in the research by Suzen et al. [13], which was referred to in the results validation section. The distance between the location of the actuator and the leading edge of the airfoil has been assumed to be 0.55C, where C denotes the chord length of the airfoil of each section. The actuator has been placed at a radius range of 0.2 m to 0.96 m along the blade.

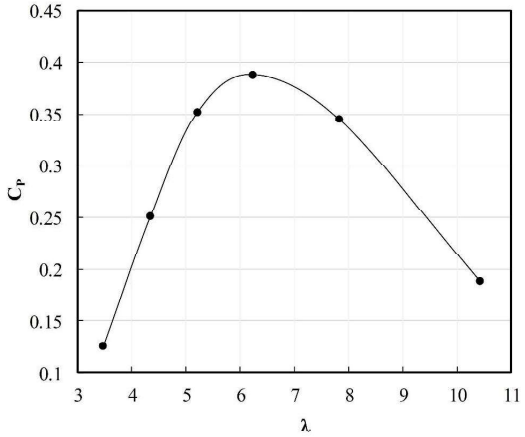

Figure 7. the power coefficient of the wind turbine at different tip speed ratios

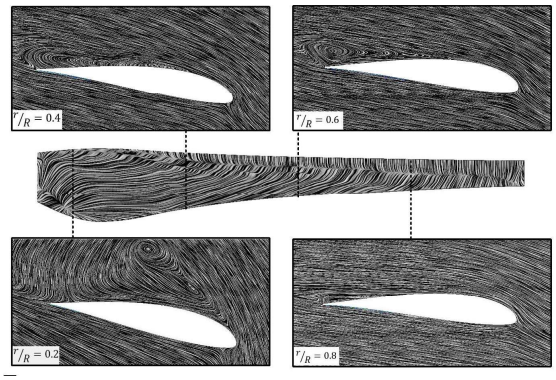

Figure 8. Streamlines over the wind turbine blade surface at $\lambda = 4{,}35$

In this research, the simulation results are presented based on $\phi^{max}\rho_c^{max}$. In the research by Suzen et al. [13], ϕ^{max} and ρ_c^{max} are taken to be 5 kV and 0.0075 C/m^3, respectively. Hence, $\phi^{max}\rho_c^{max}$ is 37.5 in the research by Suzen et al. [13]. In the simulations conducted in the present research, $\phi^{max}\rho_c^{max}$ has been considered as 37.5, 375, and 3750. Although $\phi^{max}\rho_c^{max}$ of 3750 is not practical, it has been used in this research for a scientific investigation of the effect of plasma actuator strength on the improvement in the performance of the wind turbine.

The values of increase in the wind turbine power at $\lambda = 4.35$ and different $\phi^{max}\rho_c^{max}$ are shown in Table 3. According to this table, the wind turbine power output has not considerably changed under conditions of $\phi^{max}\rho_c^{max} = 37.5$, whereas it has

increased up to 29% with an increase in $\phi^{max}\rho_c^{max}$ to 3750.

Table 3. Turbine power increasing by activating DBD plasma actuator at $\lambda = 4.35$

$\phi^{max}\rho_c^{max}$	37.5	375	3750
Power increasing (%)	0.33	8.05	29.09

Fig. 9 displays the surface streamlines over the wind turbine blade and the flow around the airfoil at the section $r/R = 0.7$ relative to $\phi^{max}\rho_c^{max}$. As shown in this figure, with an increase in $\phi^{max}\rho_c^{max}$, the plasma actuator has a greater effect on eliminating span-wise flows. For $\phi^{max}\rho_c^{max} = 3750$ conditions over large areas of the wind turbine blade, the flow has no separation, and a two-dimensional flow along the chord exists. In general, the higher the value of $\phi^{max}\rho_c^{max}$ reaches, the closer the point of flow separation to the trailing edge will get, and the smaller the secondary flows will become.

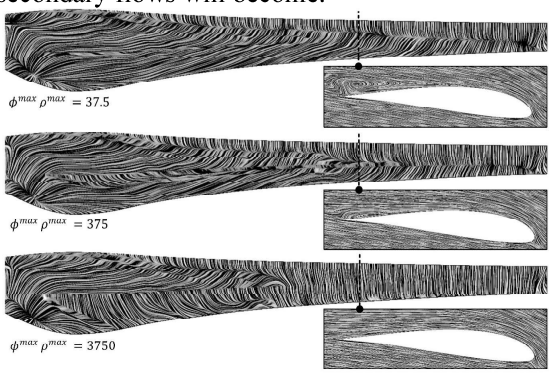

Figure 9. Effects of the plasma actuator on the surface streamlines over the wind turbine blade at $\lambda = 4{,}35$

Fig. 10 displays the distribution of the torque generated by different sections of the wind turbine relative to $\phi^{max}\rho_c^{max}$. As seen in this figure, in the regions $r/R = 0.4 - 0.95$, a difference in the generated torque can be observed for active and inactive plasma modes, and the plasma actuator has not significantly affected the generated torque in the other sections. This conclusion can also be predicted from the streamlines presented in Fig. 9. As seen in this figure, as one approaches the root of the wind turbine blade, the effect of the plasma actuator on the streamlines at the turbine blade surface is decreased.

Given that the chord lengths of the airfoils near the roots of the wind turbine blade are larger than those near the tip of the blade, a larger force is required to improve the flow in the former regions. Therefore, one of the reasons for the insignificant performance of the plasma actuator near the root of the wind turbine blade is the larger size of the airfoils of the blade at these locations.

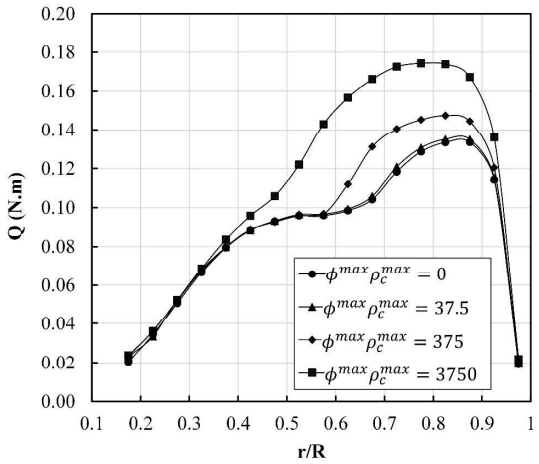

Figure 10. Distribution of the torque generated by different sections of the wind turbine blade at $\lambda = 4.35$.

The location of the plasma actuator affects the aerodynamic performance of the wind turbine. The approximate distance of the separation point from the plasma actuator location (Δx) at each section of the wind turbine blade was computed. This distance has been made dimensionless in terms of the chord length of the airfoil on which the actuator is placed and has been expressed as $\Delta x/C$. If the location of the actuator is after the separation point, this parameter is positive, and if the actuator location is before the separation point, this parameter is negative. In this research, $\Delta x/C$ is negative for the airfoils near the tip of the wind turbine and increases as one approaches the blade root.

Moreover, the ratio of increase in the torque generated by each blade section due to the activation of the plasma actuator to the torque generated by each section in the plasma-off mode is denoted as $\Delta Q/Q_0$. Fig. 11 shows variations in the torque generated by the sections of the wind turbine blade versus the distance of the actuator from the separation point. Due to the small change of output power in $\phi^{max}\rho_c^{max} = 37.5$, this case is not expressed in this figure. As seen in this figure, the behavioral pattern of the graph for the modes

with $\phi^{max}\rho_c^{max}$ equal to 375 and 3750 are similar. When $\Delta x/C \simeq 0.2$, the largest increase in torque due to the plasma actuator occurs. These regions correspond to $r/R = 0.5 - 0.7$. The maximum increase in the torque generated by the airfoils due to the activation of the plasma actuator for the modes with $\phi^{max}\rho_c^{max}$ of 375 and 3750 is 25.8% and 59.4%, respectively.

In the case of $\phi^{max}\rho_c^{max} = 375$ when $\Delta x/C$ is in the range of 0.25 to 0.4 the effect of plasma actuator on the output torque can be neglected. $\Delta x/C = 0.25 - 0.4$ corresponds to $r/R = 0.3 - 0.6$. Comparing Figures 8 and 9, when $\phi^{max}\rho_c^{max} = 375$, the plasma actuator in the range of the mentioned radii was not able to significantly change the separation position and the flow pattern on the blade. According to Figure 11, the distance of the plasma actuator from the separation point is very important in increasing the wind turbine production. This optimal distance is also a function of the value of $\phi^{max}\rho_c^{max}$.

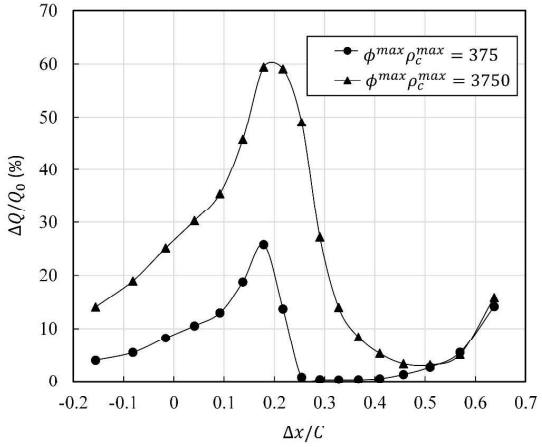

Figure 11. Variations in the torque generated by the blade sections versus the distance of the actuator from the separation point

Conclusion

In this research, the performance of the DBD plasma actuator on a small wind turbine has been studied. The studied wind turbine has a diameter of 1.93 m, and the plasma actuator has been placed span-wise at a distance of 0.55C from the leading edge. At first, the power generated by this wind turbine without the plasma actuator was derived at different tip speed ratios. The maximum power generated by this turbine occurs at a tip speed ratio of about 6. To examine the effect of the plasma actuator, $\lambda = 4.35$, which has a low power coefficient, was selected. At this tip speed ratio, three-dimensional flows dominate over the wind turbine blade, and separation occurs near the leading edge.

With the activation of the plasma actuator, the separation point moves away from the leading edge, and a chord-wise two-dimensional flow dominates over the blade. These factors cause an increase in the power output. The amount of increase in power depends on the power of the actuator. The changes in the generated power due to the activation of the plasma actuator for $\phi^{max}\rho_c^{max}$ of 37.5, 375, and 3750 are 0.33%, 8.05%, and 29.09%, respectively. The maximum increase in the torque resulting from the activation of the plasma actuator occurs at the radius range of $r/R = 0.5 - 0.7$. In these regions, the distance between the separation point and the plasma actuator location is about 0.2C.

Data Availability

All data, models, or codes that support the findings of this study are available from the corresponding author upon reasonable request.

References

[1] A. Zervos and R. Adib, "Renewables 2018 global status report," *Paris: REN21 Secretariat REN21,* 2018.

[2] P. Clausen and D. Wood, "Recent advances in small wind turbine technology," *Wind Engineering,* vol. 24, no. 3, pp. 189-201, 2000.

[3] E. J. N. Menezes, A. M. Araújo, and N. S. B. da Silva, "A review on wind turbine control and its associated methods," *Journal of cleaner production,* vol. 174, pp. 945-953, 2018.

[4] S. Rehman, M. Alam, L. Alhems, and M. Rafique, "Horizontal axis wind turbine blade design methodologies for efficiency enhancement—A Review," *Energies,* vol. 11, no. 3, p. 506, 2018.

[5] M. Akhter and F. K. Omar, "Review of Flow-Control Devices for Wind-Turbine Performance Enhancement," *Energies,* vol. 14, no. 5, p. 1268, 2021.

[6] U. Seth ,P. Traoré, F. Duran-Olivencia, E. Moreau, and P. Vazquez, "Parametric study of a DBD plasma actuation based on the Suzen-Huang model," *Journal of Electrostatics,* vol. 93, pp. 1-9, 2018.

[7] J. Kriegseis, B. Simon, and S. Grundmann, "Towards in-flight applications? a review on dielectric barrier discharge-based boundary-layer control," *Applied Mechanics Reviews,* vol. 68, no. 2, p. 020802, 2016.

[8] M. Kotsonis, "Diagnostics for characterisation of plasma actuators," *Measurement Science and Technology,* vol. 26, no. 9, p. 092001, 2015.

[9] N. Benard and E. Moreau, "Electrical and mechanical characteristics of surface AC dielectric barrier discharge plasma actuators applied to airflow control," *Experiments in Fluids,* vol. 55, no. 11, p. 1846, 2014.

[10] J. Jacob, R. Rivir, C. Carter, and J. Estevadeordal, "Boundary layer flow control using AC discharge plasma actuators," in *2nd AIAA Flow Control Conference*, 2004, p. 2128 .

[11] Y. Suzen, G. Huang, J. Jacob, and D. Ashpis, "Numerical simulations of plasma based flow control applications," in *35th AIAA Fluid Dynamics Conference and Exhibit*, 2005, p. 4633 .

[12] Y. Suzen and G. Huang, "Simulations of flow separation control using plasma actuators," in *44th AIAA Aerospace Sciences Meeting and Exhibit*, 2006, p. 87 .

[13] Y. Suzen, G. Huang, and D. Ashpis, "Numerical Simulations of Flow Separation Control in Low-Pressure Turbines Using Plasma Actuators " in *45th AIAA Aerospace Sciences Meeting and Exhibit*, Reno, Nevada., 2007 .

[14] I. Halimi Bin Ibrahim and M. Skote, "Effects of the scalar parameters in the Suzen-Huang model on plasma actuator characteristics," *International Journal of Numerical Methods for Heat & Fluid Flow,* vol. 23, no. 6, pp. 1076-1103, 2013.

[15] C. L. Enloe *et al.*, "Mechanisms and responses of a dielectric barrier plasma actuator: Geometric effects," *AIAA journal,* vol. 42, no. 3, pp. 595-604, 2004.

[16] F. O. Thomas, T. C. Corke, M. Iqbal, A. Kozlov, and D. Schatzman, "Optimization of dielectric barrier discharge plasma actuators for active aerodynamic flow control," *AIAA journal,* vol. 47, no. 9, pp. 2169-2178, 2009.

[17] A. R. Hoskinson, N. Hershkowitz, and D. E. Ashpis, "Force measurements of single and double barrier DBD plasma actuators in quiescent air," *Journal of Physics D: Applied Physics,* vol. 41, no. 24, p. 245209, 2008.

[18] J. Kriegseis, B. Möller, S. Grundmann, and C. Tropea, "Capacitance and power consumption quantification of dielectric barrier discharge (DBD) plasma actuators," *Journal of Electrostatics,* vol. 69, no. 4, pp. 302-312, 2011.

[19] H. Hoeijmakers and J. Meijerink, "Plasma actuators for active flow control on wind turbine blades," in *29th AIAA Applied Aerodynamics Conference*, 2011, p. 3353 .

[20] M. Tanaka, N. Kubo, and H. Kawabata, "Plasma actuation for leading edge separation control on 300-kW rotor blades with chord length around 1 m at a Reynolds number around 1.6× 106," in *Journal of Physics: Conference Series*, 2020, vol. 1618, no. 5: IOP Publishing, p. 052013 .

[21] J. A. Cooney, C. Szlatenyi, and N. E. Fine" ,The development and demonstration of a plasma flow control system on a 20 kW wind turbine," in *54th AIAA Aerospace Sciences Meeting*, 2016, p. 1302 .

[22] T. N. Jukes, "Smart control of a horizontal axis wind turbine using dielectric barrier discharge plasma actuators," *Renewable Energy,* vol. 80, pp. 644-654, 2015.

[23] H. Matsuda *et al.*, "Plasma Actuation Effect on a MW class Wind Turbine," *International Journal of Gas Turbine, Propulsion and Power Systems,* vol. 9, no. 1, 2017.

[24] A. Ebrahimi and M. Movahhedi, "Power improvement of NREL 5-MW wind turbine using multi-DBD plasma actuators," *Energy Conversion and Management,* vol. 146, pp. 96-106, 2017.

[25] J. Omidi and K. Mazaheri, "Improving the performance of a numerical model to simulate the EHD interaction effect induced by dielectric barrier discharge," *International Journal of Heat and Fluid Flow,* vol. 67, pp. 79-94, 2017.

[26] J. Omidi and K. Mazaheri, "Aerodynamic Enhancement and Improving the Performance of a Six-Megawatt DOWEC Wind Turbine by Micro-Plasma Actuator," *International Journal of Mechanical Sciences,* vol. 195, p. 106228, 2021.

[27] D. Wood, "Small wind turbines," in *Advances in wind energy conversion technology*: Springer, 2011, pp. 195-211.

[28] A. K. Wright and D. H. Wood, "The starting and low wind speed behaviour of a small horizontal axis wind turbine," *Journal of Wind Engineering and Industrial Aerodynamics,* vol. 92, pp. 1265–1279, 2004.

[29] D. H. Wood, "A Blade Element Estimation of the Cut-in Wind Speed of a Small T urbine " *Wind Engineering,* vol. 25, no. 4, pp. 249–255, 2001.

[30] D. Wood and T. Robotham, "Design and Testing of High Performance Blades for a600 Watt Horizontal-axis Wind Turbine " presented at the Proceedings of the 1999 Australian Wind Energy Conference 1999.

[31] P.D. Clausen, P. Freere, P. Peterson, S. V. R. Wilson, and D. H. Wood, "The Shape and Performance of Hand-Carved Small Wind Turbine Blades," *Wind Engineering,* vol. 33, no. 3, pp. 299-304, 2009.

[32] P. R. Ebert and D. H. Wood, "Oservation Of The Starting Behavior Of a Small Horizontal- Axis Wind Turbine," *Renewable Energy,* vol. 12, no. 3, pp. 245-257, 1997.

[33] J. D. Jacob, K. Ramakumar, R. Anthony, and R. B. Rivir, "Control of laminar and turbulent shear flows using plasma actuators," in *4th International Symposium on Turbulence and Shear Flow Phenomena*, Williamsburg, 2005 .